Available online at www.sciencedirect.com
ScienceDirect
International Journal of Heat and Mass Transfer 50 (2007) 2675–2691
International Journal of HEAT and MASS TRANSFER
www.elsevier.com/locate/ijhmt

Evaporation of droplets into a background gas: Kinetic modelling

S.S. Sazhin [a,*], I.N. Shishkova [b], A.P. Kryukov [b], V.Yu. Levashov [b], M.R. Heikal [a]

[a] School of Engineering, Faculty of Science and Engineering, University of Brighton, Cockcroft Building, Brighton BN2 4GJ, UK
[b] Low Temperature Department, Centre of High Technologies, Moscow Power Engineering Institute, Krasnokazarmennaya 14, Moscow 111250, Russia

Received 22 June 2006
Available online 6 March 2007

Abstract

A new kinetic model for droplet evaporation into a high pressure background gas, approximated by air, is described. Two regions above the surface of the evaporating droplet are considered. These are the kinetic region, where the analysis is based on the Boltzmann equation, and the hydrodynamic region. It is assumed that the mass fluxes leaving the kinetic region and the corresponding diffusion fluxes in the hydrodynamic region are matched. A modified version of the previously developed method of direct numerical solution of the Boltzmann equation is used. It is assumed that the mass flux leaving the droplet's surface is the maximal one (evaporation coefficient is equal to 1). The model and numerical algorithm allowed us to calculate the value of the net evaporation coefficient, defined as the ratio of the actual mass flux leaving the kinetic region and the maximal possible mass flux. The values of this coefficient for diesel fuel (approximated by *n*-dodecane) were shown to be much less than 1 for droplet surface temperatures less than 650 K. For these droplets, the kinetic effects predicted by the new model turned out to be negligible when the contribution of air in the kinetic region was ignored. These effects, however, appear to be noticeable, and larger than those predicted by the approximate analysis, if the contribution of air in the kinetic region is taken into account. It is recommended that the kinetic effects are taken into account when accurate analysis of diesel fuel droplet evaporation is essential.

Keywords: Evaporation; Diesel fuel; Droplets; *n*-dodecane; Kinetic modelling; Binary mixture

1. Introduction

Since the pioneering papers by Hertz [1] and Knudsen [2] the kinetic methods have been widely used in the modelling of evaporation, condensation and other transfer processes (e.g. [3–10]). These methods have been almost exclusively applied to the cases when gases are rarefied with Knudsen numbers (Kn) exceeding 10^{-2}. At the same time, a number of authors drew attention to the fact that, even in the case where $Kn \to 0$, the application of hydrodynamic methods to modelling fluid dynamics and heat and mass transfer processes is not always justified [11–16]. In the recent paper by Kryukov et al. [17] it was demonstrated that even in the case of droplet evaporation into a high pressure gas (diesel engines) the kinetic effects may not be negligible. It was shown that these effects can lead to increases in the evaporation time by up to 5–10%, compared with the prediction of the conventional hydrodynamic model in the case of small droplets (radii about 5 μm) injected into a hot gas with temperatures $T_g = 750$–2000 K. The hydrodynamic models for droplet evaporation are essentially based on the assumption that molecules can be removed from the surface of the droplets quickly enough to maintain fuel vapour concentration near the droplets at the saturation level [18,19]. The kinetic models take into account the fact that the speed of removal of these molecules can be insufficient to maintain the concentration of vapour at this level. Hence, the evaporation rate predicted by hydrodynamic models is always larger when compared with the rate predicted by kinetic models.

Although the kinetic processes take place mainly in a very thin Knudsen layer adjacent to the droplet surface, a

* Corresponding author. Tel.: +44 01273 642300; fax: +44 01273 642301.
E-mail address: S.Sazhin@brighton.ac.uk (S.S. Sazhin).

0017-9310/$ - see front matter © 2007 Elsevier Ltd. All rights reserved.
doi:10.1016/j.ijheatmasstransfer.2006.11.043

Nomenclature

a, b	coefficients introduced in Eq. (21)
a_{press}	parameter introduced in Eq. (8)
$\tilde{a}$	coefficient introduced in Eq. (23)
B_M	Spalding mass number
B_T	Spalding temperature number
D	binary diffusion coefficient
f	molecular velocity distribution function
E	relative error
h	convection heat transfer coefficient
j	mass flux
J	collision integral
k	thermal conductivity
k_{B}	Boltzmann constant
Kn	Knudsen number
K_0	parameter introduced in Eq. (18)
Le	Lewis number
m	mass
M	molar mass
n	number density
$\mathbf{n}_0$	unit vector
N	$\delta_{R_{\text{d}}}/\lambda_{\text{c}}$
N_{A}	Avogadro number
$N_{\alpha\beta}^{k,n-1}$	parameter introduced by Eq. (16)
Q	heat rate
p	pressure or probability density function
$\mathbf{r}$	radius-vector
R	$R_{\text{d}}/R_{\text{d0}}$
$R_{\text{v(a)}}$	gas constant referring to fuel vapour (air)
R_{d}	droplet radius
R_{u}	universal gas constant
t	time
T	temperature (with subscript) or $T_{\text{s}}/T_{\text{cr}}$ (without subscript)
T^*	$k_{\text{B}}T_{\text{r}}/\varepsilon_{\text{va}}$
$\mathbf{v}$	velocity
V	volume in the five-dimensional space
$V^{\text{l(g)}}$	specific volume of liquid (gas)
$\mathbf{w}$	vector in the five-dimensional space ($\mathbf{v}_{\beta l}, \theta_l, \phi_l$)
x	distance from the droplet surface
Y	mass fraction

Greek symbols

β	evaporation coefficient
β_{e}	net evaporation coefficient
$\delta_{R_{\text{d}}}$	thickness of the kinetic region
Δp	grid size in the momentum space
ε_{va}	$\sqrt{\varepsilon_{\text{v}}\varepsilon_{\text{a}}}$
$\varepsilon_{\text{v}}, \varepsilon_{\text{a}}$	Lennard-Jones parameters for fuel vapour and air
θ	angular coordinate
$\kappa_{R_{\text{d}}}$	coefficient introduced in Eq. (11)
λ_{c}	mean free path
$\nu_{\alpha\beta}^{k,n-1}$	parameter introduced by Eq. (16)
ρ	density
σ	diameter of molecules
σ_{eff}	effective diameter of molecules
τ_{evap}	evaporation time
ϕ	angular coordinate
$\Omega_{\text{D,va}}$	parameter introduced in Formula (12)

Subscripts

a	air
α, β	$\alpha = \text{a, v}$; $\beta = \text{a, v}$
c	frame of reference linked with the centre of inertia
cr	critical
d	droplet
e	evaporation
diff	diffusion
g	gas
l	liquid
mix	mixture
M	molecules
N_2	nitrogen
p	constant pressure
r, ref	reference
Rd	outer boundary of the kinetic region
s	surface
v	fuel vapour
x, y, z	Cartesian coordinates
0	initial

Superscripts

k	position of a velocity cell
M	total number of cells or model under consideration
n	consecutive time steps
RK	rigorous kinetic
$'$	after the collision
$\sim$	after the first step or normalised
$+$	away from the droplet
$-$	towards the droplet

noticeable reduction of the density of vapour is observed between the surface of the droplet and the outer boundary of this layer. In this case, the flux density of vapour, as predicted by the kinetic model, is controlled by the vapour density at the outer boundary of the Knudsen layer. The latter is less than the vapour density at the droplet surface, which controls the vapour flux predicted by the hydrodynamic model. This is consistent with the above mentioned conclusion regarding the evaporation rates predicted by kinetic and hydrodynamic models.

The kinetic model for diesel fuel droplet evaporation used in [17] was essentially based on the analysis reported earlier in [20]. This was an approximate analysis of the Boltzmann equation, performed under a number of assumptions and leading to an explicit expression for mass flux of vapour leaving the droplet. Two of these assumptions seem to be particularly important for practical applications. These are the assumption that the evaporation coefficient β is a priori given and the assumption that no other gases, apart from vapour, are present in the vicinity of the droplet surface. The evaporation coefficient is defined as the ratio of the actual mass flux leaving the surface of the droplet (before the first collision) j_{es} and the maximal possible flux

$$\beta = \frac{j_{es}}{\rho_{vs}\sqrt{\frac{R_v T_s}{2\pi}}}, \tag{1}$$

where ρ_{vs} is the density of saturated fuel vapour corresponding to the liquid temperature at the droplet surface, $T_s = T_{ls}$, R_v is the gas constant for fuel vapour. Since no direct measurements or calculations of β for diesel fuel were available when paper [17] was prepared, the minimal and average values of this parameter for water (0.04 and 0.5) were used. The second assumption can hardly be justified in the case of diesel fuel droplet evaporation into high pressure air [21,22].

Quantitative analysis of evaporation and condensation processes in binary mixtures seems infeasible in the approach used in [17]. In [16] the two-surface problems of a multicomponent mixture of vapour and non-condensable gases in the continuum limit were studied based on asymptotic analysis of the Boltzmann equation. An asymptotic analysis of the linearised Boltzmann equation for the binary mixture was presented in [23].

The approach used in this paper is based on the application of numerical methods, such as those developed in [24–26]. The numerical analysis of the Boltzmann equation has been previously undertaken by several authors and the results have been reported in a number of papers, including [27–29]. In all these papers, however, it was assumed that the sizes of all molecules in binary mixtures are the same. This is hardly justified in the case of diesel fuel evaporation into a high pressure air, when the effective radius of fuel ($C_{12}H_{26}$) molecules is about 2.5× larger than the effective radius of air (N_2) molecules. This was the main driving force behind the development of a new numerical algorithm, specifically designed to model the evaporation and condensation processes in binary mixtures consisting of molecules with different radii and masses [30,31]. In the present study, this algorithm is applied to the same problem of evaporation of diesel fuel into a high pressure air, as considered earlier in [17]. The results of calculations using this algorithm are compared with the prediction of the hydrodynamic model and the approximate model used in [17]. The results of this comparison allow us to reach reliable conclusions regarding the range of applicability and accuracy of the hydrodynamic model of droplet evaporation, and the approximate kinetic model used in [17].

The physical model is described in Section 2. In Sections 3 and 4 the numerical algorithm is briefly described. The results of calculations of diesel fuel droplet heating and evaporation (using the new model and numerical algorithm, the hydrodynamic model and the simplified model used in [17]) are presented in Section 5. The main results of the paper are summarised in Section 6.

2. Model

As in [17], we consider two regions of gas above the surface of the evaporating fuel droplet; the kinetic region and the hydrodynamic region. These are schematically shown in Fig. 1. In contrast to [17], however, we assume that gas consists of two components, fuel vapour and background gas, both in the kinetic region and in the hydrodynamic region. The background gas is identified with air, assuming that the contribution of chemical reactions of fuel vapour and oxygen can be ignored. Fuel vapour and air dynamics in the first region are described by the Boltzmann equations, while the conventional hydrodynamic analysis is applied in the second region. That means that we investigate a two surface problem, similar to the one considered in [16,27]. The location of the boundary between these regions is determined based on a separate analysis to be discussed later, in Section 4. It is expected to be about 10–1000 mean molecular free paths from the droplet surface.

2.1. Kinetic region

The evolution of the molecular velocity distribution functions of air $f_a \equiv f_a(\mathbf{r}, t, \mathbf{v})$ and fuel vapour $f_v \equiv f_v(\mathbf{r}, t, \mathbf{v})$

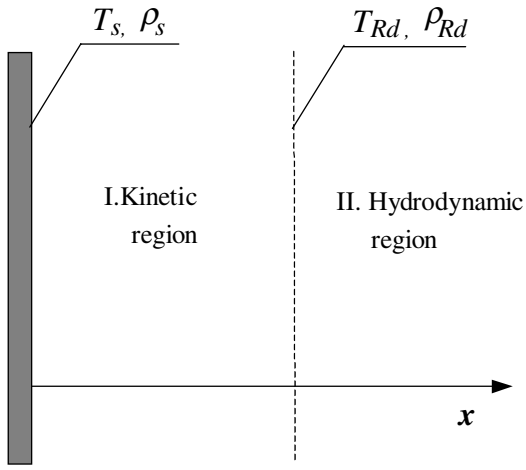

Fig. 1. Kinetic and hydrodynamic regions above the surface of the droplet. T_s is the droplet surface temperature, ρ_s is the fuel vapour density in the immediate vicinity of the droplet surface, T_{Rd} and ρ_{Rd} are the temperature and density of fuel vapour at the outer boundary of the Knudsen region.

in the kinetic region is controlled by the corresponding Boltzmann equations [32]

$$\left.\begin{aligned}\frac{\partial f_{\mathrm{a}}}{\partial t}+\mathbf{v}_{\mathrm{a}}\frac{\partial f_{\mathrm{a}}}{\partial \mathbf{r}}&=J_{\mathrm{aa}}+J_{\mathrm{av}},\\ \frac{\partial f_{\mathrm{v}}}{\partial t}+\mathbf{v}_{\mathrm{v}}\frac{\partial f_{\mathrm{v}}}{\partial \mathbf{r}}&=J_{\mathrm{va}}+J_{\mathrm{vv}},\end{aligned}\right\} \tag{2}$$

where $J_{\alpha\beta}$ ($\alpha=\mathrm{a},\mathrm{v};\ \beta=\mathrm{a},\mathrm{v}$) are collision integrals defined as

$$J_{\alpha\beta}=\frac{\sigma_{\alpha\beta}^2}{2}\int_{-\infty}^{+\infty}\mathrm{d}\mathbf{v}_1\int_0^{\pi}\sin\theta\,\mathrm{d}\theta\int_0^{2\pi}\mathrm{d}\phi\,(f'_{\alpha}f'_{\beta 1}-f_{\alpha}f_{\beta 1})|\mathbf{v}_{\alpha}-\mathbf{v}_{\beta 1}|, \tag{3}$$

$\sigma_{\alpha\beta}=(\sigma_{\alpha}+\sigma_{\beta})/2$, σ_{α} and σ_{β} are the corresponding diameters of molecules, θ and ϕ are angular coordinates of molecules β relative to molecules α after the collision, superscript ′ indicates the velocities and the molecular velocity distribution functions after collisions (in what follows these functions will be referred to as 'molecular distribution functions'). Subscript 1 indicates that molecules of type β collide with molecules of type α and as a result of this interaction the function f_{α} is modified. The first integral in the right-hand side of (3) is calculated in the three dimensional velocity space. When deriving (2) and (3) it was assumed that molecules are rigid elastic spheres and body forces acting on them are negligible.

Note that the approximation of the collisions involving *n*-dodecane molecules as elastic can be crude. The rigorous analysis of inelastic collisions, when calculating collision integrals, would have required the application of kinetic methods taking into account transfer of energy between rotational, vibrational and translational degrees of freedom of individual molecules [33]. Difficulties of this approach, even at the level of formulation of reliable equations, are well known [34,35]. Since the new level of complexity of the two-surface evaporation–condensation problem in the presence of a non-condensable component has been introduced in our paper, these effects of non-elastic collisions were not included in our analysis. Possible approximation of molecules to rigid spheres in this case is merely our conjecture, which we believe to be acceptable at the first stage of investigating this problem.

In order to calculate the integral in (3), one needs to know the molecular distribution functions f'_{α} and $f'_{\beta 1}$ after collisions. To do this, it is necessary to establish the relationship between $\mathbf{v}_{\alpha}$, $\mathbf{v}_{\beta 1}$ on one side and $\mathbf{v}'_{\alpha}$, $\mathbf{v}'_{\beta 1}$ on the other side. Remembering our assumption that collisions are elastic, the laws of conservation of momentum and energy lead to the following system of equations for $\mathbf{v}'_{\alpha}$ and $\mathbf{v}'_{\beta 1}$ [36]:

$$\left.\begin{aligned}\mathbf{v}'_{\alpha}&=\frac{m_{\beta}}{m_{\alpha}+m_{\beta}}|\mathbf{v}'_{\alpha}-\mathbf{v}'_{\beta 1}|\mathbf{n}_0+\frac{m_{\alpha}\mathbf{v}_{\alpha}+m_{\beta}\mathbf{v}_{\beta 1}}{m_{\alpha}+m_{\beta}},\\ \mathbf{v}'_{\beta 1}&=-\frac{m_{\alpha}}{m_{\alpha}+m_{\beta}}|\mathbf{v}'_{\alpha}-\mathbf{v}'_{\beta 1}|\mathbf{n}_0+\frac{m_{\alpha}\mathbf{v}_{\alpha}+m_{\beta}\mathbf{v}_{\beta 1}}{m_{\alpha}+m_{\beta}},\end{aligned}\right\} \tag{4}$$

where m_{α} and m_{β} are the masses of molecules, $\mathbf{n}_0$ is the unit vector in the direction of molecular velocity after the collision in the frame of reference linked with the centre of inertia of colliding molecules.

The initial molecular distribution functions of both vapour and air molecules are assumed to be Maxwellian

$$f_{\mathrm{a,v}}=n_{\mathrm{a,v}}\left(\frac{1}{2\pi R_{\mathrm{a,v}}T_{\mathrm{s}}}\right)^{3/2}\exp\left(-\frac{v_x^2+v_y^2+v_z^2}{2R_{\mathrm{a,v}}T_{\mathrm{s}}}\right), \tag{5}$$

where $n_{\mathrm{a,v}}$ are number densities of air and fuel vapour molecules, $R_{\mathrm{a,v}}$ are gas constants of air and fuel vapour, T_{s} is assumed to be the same for air and fuel vapour,

$$n_{\mathrm{a,v}}=\frac{\rho_{\mathrm{a,v}}}{M_{\mathrm{a,v}}}N_{\mathrm{A}}=\frac{p_{\mathrm{a,v}}}{R_{\mathrm{u}}T_{\mathrm{s}}}N_{\mathrm{A}}, \tag{6}$$

$\rho_{\mathrm{a,v}}$ are the densities of air and vapour, $M_{\mathrm{a,v}}$ are molar masses of air and vapour (kg/kmol), R_{u} is the universal gas constant, N_{A} is the Avogadro constant, p_{v} and p_{a} are the partial pressures of fuel vapour and air ($p_{\mathrm{a}}=p_{\mathrm{total}}-p_{\mathrm{v}}$).

The Boltzmann equation is solved in the kinetic region assuming that the droplet surface and the surface of the outer boundary of this region are flat. The effects of the curvature of the surface of the droplet are taken into account when calculating the fluxes at its outer boundary. It is assumed that at the surface of the droplet the molecular distribution functions of fuel vapour and air are maintained Maxwellian for $v_x\geqslant 0$ with

$$n_{\mathrm{vs}}=\beta\frac{p_{\mathrm{vs}}}{R_{\mathrm{u}}T_{\mathrm{s}}}N_{\mathrm{A}}, \tag{7}$$

where β is the evaporation coefficient defined by Eq. (1).

The droplet surface is not transparent for air molecules. Also, the molecular distribution functions of fuel vapour and air at the outer boundary of the kinetic region are assumed to be Maxwellian for $v_x\leqslant 0$ with

$$n_{\mathrm{vRd}}=\frac{p_{\mathrm{vRd}}}{R_{\mathrm{u}}T_{\mathrm{s}}}N_{\mathrm{A}}\quad\text{and}\quad n_{\mathrm{aRd}}=\frac{p_{\mathrm{aRd}}}{R_{\mathrm{u}}T_{\mathrm{s}}}N_{\mathrm{A}},$$

where p_{vRd} and p_{aRd} are the partial pressures of fuel vapour and air at the outer boundary of the kinetic region. The additional subscripts s and Rd indicate the droplet surface and the outer boundary of the kinetic region. It is assumed that the fluxes of air to and away from the surface of the droplet are equal. Note that although the kinetic model predicts a small drop in the partial pressure of vapour between the surface of the droplet and the outer boundary of the kinetic region, the effect of this drop on the partial pressure of air was shown to be small (less than 1%) and is ignored in our analysis.

The vapour and air temperatures at the outer boundary of the kinetic region are assumed equal to that at the surface of the droplet: $T_{\mathrm{Rd}}=T_{\mathrm{s}}$. This assumption can be justified by small thickness of the kinetic region. One of the first attempts to relax this assumption and solve the problems of simultaneous heat and mass transfer in binary mixtures was reported in [37]. A more detailed analysis of this issue is not straightforward. It is beyond the scope of this paper.

Assuming that fuel vapour leaving the droplet surface is saturated *n*-dodecane vapour, and using data presented in [38], the following approximation can be obtained:

$$p_{vs} = p_{ref} \exp\left[\frac{T_s - T_{ref}}{a_{pres}}\right], \tag{8}$$

where

$$\left.\begin{array}{l} p_{ref} = 70.44 \text{ Pa}; \quad T_{ref} = 300.18 \text{ K}; \quad a_{pres} = 22.37 \text{ K} \\ \quad \text{when } T_s \leqslant 440.00 \text{ K}, \\ p_{ref} = 46204.48 \text{ Pa}; \quad T_{ref} = 449.87 \text{ K}; \quad a_{pres} = 56.97 \text{ K} \\ \quad \text{when } T_s > 440.00 \text{ K}. \end{array}\right\}$$

Note that the mass fraction of fuel vapour can be estimated as

$$Y_{vs} = \left[1 + \left(\frac{p}{p_{vs}} - 1\right)\frac{M_a}{M_v}\right]^{-1}, \tag{9}$$

where p is the total pressure of the mixture of fuel vapour and air.

Exactly the same boundary condition for p_v is used in hydrodynamic models of droplet evaporation, where the evaporation problem is reduced to the problem of diffusion and convection of vapour outside droplets. In the case of our model, however, the diffusion and convection of vapour takes place not from the surface of the droplet but from the outer boundary of the kinetic region.

Note that the values of Y_{vs}, n_{vs}, ρ_{vs} and p_{vs} refer only to fuel vapour molecules leaving the surface of the droplet. In the general case, these values are different from the actual mass fraction, number density, mass density and partial pressure, which take into account the contribution of both outgoing and incoming molecular fluxes. The latter are obtained from the solution of the Boltzmann equation in the kinetic region. The partial pressure of air in the kinetic region is calculated as the difference between the total pressure and the actual partial pressure of the fuel vapour.

As mentioned in Section 1, the theoretical or experimental estimation of the evaporation coefficient used in (7) is not trivial. In most cases it can be assumed that the system is in the state of equilibrium when the evaporation coefficient coincides with the condensation coefficient. The rigorous theoretical estimation of both coefficients would require the application of molecular dynamics methods [10,39,40]. Perhaps one of the most advanced molecular dynamics investigations of these coefficients for water was reported in [40]. In this paper, two models for intermolecular potential were used: the Carravetta–Clementi model [41] and the extended simple point charge model [42]. In both models, the intermolecular interactions are treated as a combination of the short-range pairwise potential of atoms and the long-range Coulombic interaction. The predictions of the extended simple point charge model were shown to be in better agreement with experimental data. It was pointed out that the translational motion is of primary importance for the evaporation/condensation process, whereas the effects of the rotational motion are insignificant. The molecular dynamic simulation data were shown to be in good agreement with the prediction of the evaporation/condensation coefficient by the transition state theory earlier developed in [43]. In the latter paper, condensation/evaporation processes at the liquid–vapour interface were considered as a kind of chemical reaction and the general theory of rate processes [44] was applied. As a result the following simple expression for the evaporation/condensation coefficient was derived:

$$\beta = \left[1 - \left(\frac{V^l}{V^g}\right)^{1/3}\right] \exp\left[-\frac{1}{2}\frac{1}{\left(\frac{V^l}{V^g}\right)^{1/3} - 1}\right], \tag{10}$$

where V^l and V^g are specific volumes of liquid and gas respectively.

Remembering that $V^l \ll V^g$ for *n*-dodecane, except when the temperatures are close to the critical temperature, we will assume in our further analysis that $\beta = 1$, unless we compare our results with those reported earlier. We appreciate that this assumption needs to be justified more rigorously, based on molecular dynamics simulations. This, however, is beyond the scope of this paper.

2.2. Hydrodynamic region

It is assumed that the mass fluxes leaving the kinetic region and the corresponding diffusion fluxes in the hydrodynamic region are matched

$$\kappa_{R_d} \int_{-\infty}^{+\infty} dv_y \int_{-\infty}^{+\infty} dv_z \int_0^{+\infty} dv_x v_x f_v(\mathbf{r}, t, \mathbf{v}) = \frac{N_A}{M_v}\frac{\rho_{mix} D_{va}}{R_d + \delta_{R_d}} \ln(1 + B_M), \tag{11}$$

where ρ_{mix} is the density of the mixture of air and vapour at the inner boundary of the hydrodynamic region ($\rho_{mix} = \rho_{vRd}/Y_{vRd}$), D_{va} is the binary diffusion coefficient (diffusion of vapour through air), $B_M = Y_{vRd}/(1 - Y_{vRd})$ is the Spalding mass number, Y_{vRd} is the fuel vapour mass fraction at the inner boundary of the hydrodynamic region, $\kappa_{R_d} = (1 + (\delta_{R_d}/R_d))^{-2}$ is the correction factor for the difference between the area of the outer surface of the kinetic region and the area of the droplet surface, δ_{R_d} is the thickness of the kinetic region. B_M takes into account the effect of the finite mass fraction of fuel vapour on the evaporation process (see Section 3.2.1 of [19] for detail).

In [17] the analysis was based on the assumption that the Lewis number (*Le*) (see [19]) is equal to 1. In our model, no assumptions about the value of *Le* are made and the binary diffusion coefficient is calculated from the following expression [45]:

$$D_{va} = 1.8583 \times 10^{-7} \sqrt{T_r^3\left(\frac{1}{M_v} + \frac{1}{M_a}\right)} \frac{1}{p\sigma_{va}^2 \Omega_{D,va}}, \tag{12}$$

where D_{va} is in m^2/s, p is in atm (1 atm $\approx 1.01 \times 10^5$ Pa), $\sigma_{va} = 0.5(\sigma_v + \sigma_a)$ is the average diameter of molecules of vapour and air (in $m \times 10^{-10}$), $\Omega_{D,va}$ is the function of $T^* \equiv k_B T_r/\varepsilon_{va}$, $\varepsilon_{va} = \sqrt{\varepsilon_v \varepsilon_a}$, ε_v and ε_a are Lennard-Jones parameters for fuel vapour and air [45], k_B is the Boltzmann constant, $T_r = T_s + \frac{1}{3}(T_g - T_s)$ is the reference temperature, T_s is the droplet surface temperature, T_g is the ambient gas temperature.

In accordance with [45] the following approximation for $\Omega_{D,va}$ could be used:

$$\Omega_{D,va} = \frac{1.06036}{T^{*0.15610}} + \frac{0.19300}{\exp(0.47635T^*)} + \frac{1.03587}{\exp(1.52996T^*)} + \frac{1.76474}{\exp(3.89411T^*)}.$$

If, in agreement with the assumptions used in the kinetic model, we assume that the molecules can be approximated as rigid spheres, this formula for $\Omega_{D,va}$ reduces to $\Omega_{D,va} = 1$ [45]. This approximation for $\Omega_{D,va}$ is used in our analysis.

Assuming that fuel vapour can be approximated by *n*-dodecane ($C_{12}H_{26}$) and air can be approximated by N_2, we took $\sigma_v = 9.37 \times 10^{-10}$ m and $\sigma_a = \sigma_{N_2} = 3.67 \times 10^{-10}$ m [46].

As in the hydrodynamic model, heat supplied to the droplet in our model is estimated as [47]

$$Q = 4\pi R_d^2 h (T_g - T_s), \tag{13}$$

where the convection heat transfer coefficient h is obtained from the equation [47]

$$h = \frac{k_{mix}}{R_d} \frac{\ln(1 + B_M)}{B_M}, \tag{14}$$

k_{mix} is the thermal conductivity of the mixture of vapour and air. In many practical applications the contribution of vapour can be ignored and the thermal conductivity of air can be approximated as [46]

$$k_a = 0.05128 + T[-0.09885 \times 10^{-3} + T(0.21157 \times 10^{-6} - 0.094686 \times 10^{-9} T)].$$

At temperatures above about 400 K, the dependence of k_a on pressure is relatively weak. An increase of pressure from 0.1 MPa to 10 MPa would lead to an increase in k_a of less than 10% [48]. To achieve consistency with the previous paper [17] we assumed that k_{mix} is equal to the average value $k_a = 0.035$ W/(m K). This is the value of k_a at atmospheric pressure and temperature close to 450 K.

The ideal gas approximation is assumed to be valid. Following [32,49], this approximation is valid when $n_M \sigma_{eff}^3 \to 0$, where n_M is the number of molecules per unit volume, σ_{eff} is the effective diameter of molecules. For air (approximated by nitrogen) at $T_g = 600$ K and ambient pressure 3 MPa, $n_M \sigma_{eff}^3 = 0.018$. For saturated *n*-dodecane at the same temperature, $n_M \sigma_{eff}^3 = 0.1$. In both cases $n_M \sigma_{eff}^3 \ll 1$, which justifies our assumption.

Note that in the kinetic model B_M is defined by Y_{vRd}, while in the hydrodynamic model it is defined by Y_{vs}. Strictly speaking B_M in Eq. (14) should have been replaced by the Spalding temperature number B_T [50,19]. This would have changed slightly the predicted rate of heating and evaporation of droplets at the expense of making the numerical algorithm more complicated. However, this improvement of the model would hardly affect the difference in the heating and evaporation of droplets predicted by kinetic and hydrodynamic evaporation models. The inclusion of B_M in this expression makes the predictions of our model compatible with those reported in [17], whose analysis was based on Eq. (14).

The effects of temperature gradients inside droplets and thermal radiation are ignored. The range of applicability of this assumption has been discussed in [51–57]. Since *n*-dodecane droplets are semi-transparent we can expect that their radiative heating would take place mainly under their surfaces rather than at their surfaces (see e.g. [58–60]), which implies that the thermal radiation would contribute to changes in droplet surface temperature indirectly. Note that these droplets can be opaque for some parts of the radiation spectrum, which would allow us to consider the radiative heating as a surface phenomenon, similar to convection [61]. The analysis of the contribution of these effects to the evaporation process is beyond the scope of this paper.

3. Numerical algorithm

The main features of the numerical algorithm used in our calculations are described in [24,31,62]. In this section these features are briefly summarised and the new elements of the algorithm are discussed.

Time and physical space are discretised as in conventional structured computational fluid dynamics (CFD) codes [63]. The discretisation in the velocity space is performed similarly to that in the physical space, replacing continuous values of $\mathbf{v}$ by a discrete set $\{\mathbf{v}^k\}^M$, where k indicates the position of a velocity cell, M is the total number of cells. A homogeneous grid was used with the following range $v_{i\max} - v_{i\min} = 7\sqrt{2R_v T_s}$, where $i = x, y, z$, R_v is the gas constant for fuel vapour, T_s is the droplet surface temperature. Twelve cells for each velocity component were considered, giving the total number of cells in the velocity space equal to $12^3 = 1728$. This grid was tested for calculation of the dimensionless Maxwellian distribution with normalised density $\bar{n} = 1$ and normalised temperature $\overline{T} = T_g/T_s = 1$. The results of the calculation gave us: $\bar{n} = 0.9999$ and $\overline{T} = 0.9998$ [31]. Hence we can conclude that the velocity grid under consideration allows us to calculate the macroscopic variables with errors much less than 1% when the distribution function of molecules is close to the Maxwellian one. In the general case, we anticipate that this error is, at worst, just less than 1%, which we find acceptable for our applications.

The boundaries of the velocity domain in v_x, v_y, v_z directions are chosen in such a way that the contribution of molecules with velocities outside this range can be ignored. For each value of $\mathbf{v}^k$ the corresponding value of f^k is specified.

This allows us to present each of Eq. (2) in a discretised form

$$\frac{\Delta f_\alpha^k}{\Delta t}+\mathbf{v}_\alpha^k\frac{\Delta f_\alpha^k}{\Delta \mathbf{r}}=J_{\alpha\alpha}^k+J_{\alpha\beta}^k, \tag{15}$$

where $k\in[1,M]$. After calculation of $J_{\alpha\beta}^k$ for each velocity cell $\mathbf{v}_\alpha^k$, the nonlinear system of integral-differential equations (2) reduces to the linear system of algebraic equations (15).

Following [24], the numerical solution of System (15) for each gas component is performed in two steps. Firstly, molecular displacements are calculated ignoring the effect of collisions ($J_{\alpha\alpha}^k=J_{\alpha\beta}^k=0$). Secondly, the collisional relaxation is calculated under the assumption of spatial homogeneity. The boundary conditions for the molecular distribution function are taken into account in the first step. The numerical solution of Eq. (15) is performed following the explicit approach, and using the Courant condition $\Delta t\ \max(|v_x|,|v_y|,|v_z|)<\min(\Delta x,\Delta y,\Delta z)$. Between 100 and 200 cells in the physical space are used, leading to errors of less than 1%.

In the second step, the displacement of molecules stops and they start colliding. Using the explicit approach, the solution of each simplified equation in System (15) in each cell in the physical space can be written as

$$f_\alpha^{k,n}=\frac{\tilde f_\alpha^{k,n-1}+\Delta t[N_{\alpha\alpha}^{k,n-1}+N_{\alpha\beta}^{k,n-1}]}{1+\Delta t[\nu_{\alpha\alpha}^{k,n-1}+\nu_{\alpha\beta}^{k,n-1}]}, \tag{16}$$

where

$$\left.\begin{aligned}\nu_{\alpha\beta}^{k,n-1}&=\tfrac{\sigma_{\alpha\beta}^2}{2}\int_{-\infty}^{+\infty}\mathrm{d}\mathbf{v}_1\int_0^\pi\sin\theta\,\mathrm{d}\theta\int_0^{2\pi}\mathrm{d}\phi\tilde f_{\beta1}^{k,n-1}|\mathbf{v}_\alpha^k-\mathbf{v}_{\beta1}^k|,\\ N_{\alpha\beta}^{k,n-1}&=\tfrac{\sigma_{\alpha\beta}^2}{2}\int_{-\infty}^{+\infty}\mathrm{d}\mathbf{v}_1\int_0^\pi\sin\theta\,\mathrm{d}\theta\int_0^{2\pi}\mathrm{d}\phi\tilde f_\alpha'^{k,n-1}\tilde f_{\beta1}'^{k,n-1}|\mathbf{v}_\alpha^k-\mathbf{v}_{\beta1}^k|,\end{aligned}\right\} \tag{17}$$

~ indicates the value of the molecular distribution function calculated in the first step, additional superscripts $n-1$ and n indicate consecutive time steps.

The calculation of integrals $\nu_{\alpha\beta}^{k,n-1}$ and $N_{\alpha\beta}^{k,n-1}$ in Eq. (16) (see Eq. (17)) turned out to be a major challenge from the point of view of CPU requirements. In our algorithm the conventional approach to calculation of these integrals is replaced by integration based on the random cubature formulae. In this case $\nu_{\alpha\beta}^{k,n-1}$ and $N_{\alpha\beta}^{k,n-1}$ are found from the following expressions:

$$\left.\begin{aligned}\nu_{\alpha\beta}^{k,n-1}&=\tfrac{V}{K_0}\tfrac{\sigma_{\alpha\beta}^2}{2}\sum_{l=1}^{K_0}\frac{\tilde f_{\beta1l}^{k,n-1}|\mathbf{v}_\alpha-\mathbf{v}_{\beta1l}|\sin\theta_l}{p(\mathbf{w}_l)},\\ N_{\alpha\beta}^{k,n-1}&=\tfrac{V}{K_0}\tfrac{\sigma_{\alpha\beta}^2}{2}\sum_{l=1}^{K_0}\frac{\tilde f_{\alpha l}'^{k,n-1}\tilde f_{\beta1l}'^{k,n-1}|\mathbf{v}_\alpha-\mathbf{v}_{\beta1l}|\sin\theta_l}{p(\mathbf{w}_l)},\end{aligned}\right\} \tag{18}$$

where V is the volume of the five-dimensional space, $\mathbf{w}_l\equiv\mathbf{w}_l(\mathbf{v}_{\beta1l},\theta_l,\phi_l)$ is an arbitrary chosen point in this space, $p(\mathbf{w}_l)$ is the value of the probability density function of the distribution of these points, K_0 is the total number of these points (assumed number of collisions in a given cell in physical and velocity spaces), and the summation is performed over all these points. In this case the relative error of calculation of $\nu_{\alpha\beta}^{k,n-1}$ and $N_{\alpha\beta}^{k,n-1}$ is proportional to $1/\sqrt{K_0}$ and does not depend on the dimension of space [24,64]. For practical calculations we assumed homogeneous distribution of $\mathbf{w}_l$, which implies that $p(\mathbf{w}_l)=1$. The practical efficiency of the application of Eq. (18) largely depends on the choice of random nodes $\mathbf{w}_l$. One of the most widely used approaches to choosing these nodes is based on the so called Korobov sequences [65–67,62]. The condition $p(\mathbf{w}_l)=1$ for these sequences is satisfied. In the case of piecewise constant functions (used in our numerical analysis) the errors of calculations using Korobov sequences are proportional to $1/K_0$. This approach is used in our algorithm. $K_0=200$ was used in the calculations, leading to possible errors of about 1%. The explicit expression for V is presented as

$$V=2\pi^2|v_{x(\max)}-v_{x(\min)}||v_{y(\max)}-v_{y(\min)}||v_{z(\max)}-v_{z(\min)}|. \tag{19}$$

The modelling of the collision processes is based on the assumption that the collisions are elastic (momentum and energy are conserved) and the directions of momenta of molecules in the coordinate system, linked with their centres of inertia, are random. The numerical implementation of this model, however, is linked with a number of difficulties. These are related to the fact that randomly chosen directions of molecular velocities after collisions are likely to lead to the values of these velocities lying between the values in the nodes of the discretised velocity space. This can eventually lead to non-conservation of momentum and energy during the collision process. In the early papers, this problem was resolved by introducing corrections to the molecular distribution function after collision [24]. Although these corrections made the system conservative, they led to additional sources of error. In the projection method, developed later in [26], the actual molecular velocities after the collisions were replaced by pairs of velocities referring to the nearest nodes. These velocities were appropriately weighted, which ensured that the conservation of momentum and energy took place during individual collisions. This, however, led to increased complexity of the algorithm.

The approach used in our algorithm is different from the ones described above. It is based on the discretisation of the velocities, not only during the description of molecular motion, but also in the analysis of the collision processes. Two colliding molecules, with velocities $\mathbf{v}$ and $\mathbf{v}_1$, enter a certain zone of interaction. We do not know the details of the collision process, but we assume that after the collision these molecules acquire new velocities $\mathbf{v}'$ and $\mathbf{v}_1'$ for which: (1) the total momentum and energy of both molecules are conserved during the collision process (collisions are elastic); (2) vectors $\mathbf{v}'$ and $\mathbf{v}_1'$ belong to an a priori chosen set of velocities.

A conservative scheme, based of a special choice of collision parameters, was earlier discussed in [68–70]. In this

scheme the velocity vectors of molecules before and after collisions were taken in the nodes of the originally discretised velocity space. Our approach has some similarities with the approaches used in [68–70]. Its practical application can best be illustrated if we consider the collision process in the frame of reference linked with the centre of inertia of both molecules, and describe the system dynamics in terms of momenta rather than velocities. In this frame of reference the momenta of oncoming molecules have equal values but opposite directions. For the two dimensional case these are schematically shown in Fig. 2, where $p_{cx} = -1.5\Delta p$ and $p_{cy} = 1.5\Delta p$, the subscript c indicates that the momentum component is taken in the frame of reference linked with the centre of inertia of both molecules, Δp is the grid size in the momentum space (assumed to be the same in all directions). It can be shown that, in the general case, the components of momenta in the frame of reference linked with the centre of inertia of colliding molecules are always integers of $0.5\Delta p$. The collision process leads to the rotation of momenta of both molecules in such a way that their absolute values remain the same, but the directions are opposite. All possible momenta satisfying these conditions lie on the circumferences shown in Fig. 2. In contrast to most previous studies of this process, we do not consider all possible values of momenta after the collision, but restrict ourselves to the cases when the components of these momenta are integers of $0.5\Delta p$. In the two-dimensional case shown in Fig. 2, these correspond to the points of intersection of the circumference with the nodes in the momentum space. In this case there are 4 such points corresponding to 4 combinations of momenta of molecules after collision. In the three-dimensional case the circumference shown in Fig. 2 turns into the surface of a sphere and the number of possible combinations of momenta after collision increases to 12. We have observed that the maximal number of these combinations in the three-dimensional space is 24 (although we cannot prove this rigorously). In the practical implementation of this model, the calculations were performed for all possible values of θ and ϕ for each collision and then the results were averaged over these variables. This is expected to improve the accuracy of the results compared with the random selection of θ and ϕ from the set of possible values of these variables.

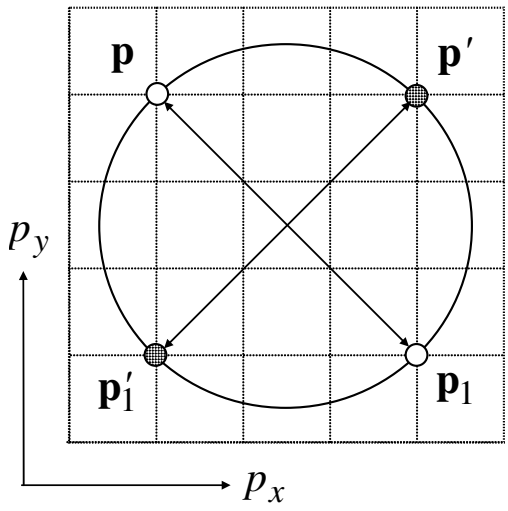

Fig. 2. Scheme of the collision process between two molecules in the frame of reference linked with their centre of inertia. $\mathbf{p}$ and $\mathbf{p}_1$ are momenta of molecules before the collision; $\mathbf{p}'$ and $\mathbf{p}'_1$ are their momenta after the collision. The sizes of the grid in this plane are assumed to be the same in p_x and p_y directions and equal to Δp. Both components of all four vectors $\mathbf{p}$, $\mathbf{p}_1$, $\mathbf{p}'$ and $\mathbf{p}'_1$ are integers of $0.5\Delta p$. The absolute values of these vectors are equal to the radii of the corresponding circumferences. The subscripts$_c$, indicating that the momenta are taken in the frame of references linked with the centre of inertia of colliding molecules, are omitted.

We believe that this approach provides consistency in discretisation processes used for the description of molecular dynamics and collision processes. It was tested on numerous problems, one of which is discussed in Section 5.

4. The matching conditions

The analysis presented so far has been based on the assumption that we know the location of the boundary between the kinetic and hydrodynamic regions. The identification of this boundary, however, proved difficult in the general case.

To illustrate the problem, we considered an example of evaporation on a *n*-dodecane ($C_{12}H_{26}$) droplet with $T_s = 600$ K, $\rho_{vs}(T_s)$ determined by Eq. (8) and ideal gas law, $T_s = T_{Rd}$ and assumed $\rho_{vRd} = 0.8\rho_{vs}$. In the following analysis the subscript v for fuel vapour will be omitted. We took the thickness of the kinetic region δ_{R_d} to be equal to $20\lambda_c$, where λ_c is the mean free path of molecules, estimated as

$$\lambda_c = \frac{1}{\sqrt{2}\pi\sigma_{N_2} n_{N_2 s}},$$

where σ_{N_2} and $n_{N_2 s}$ are the diameter of nitrogen molecules and their number density at the droplet surface, estimated at $T_s = T_{s0} = 600$ K and pressure 3 MPa. This parameter was introduced for normalising the thickness of the Knudsen region. It is not used in our calculations.

Two cases have been considered. Firstly, we assumed that there was no air in this region. Secondly, we assumed that the total pressure of the mixture of vapour and air in this region was equal to 3 MPa. The plots of ρ/ρ_s versus x/λ_c (where x is the distance from the droplet surface) for both cases are shown in Fig. 3.

As can be seen from this figure, in the case when there is no air in the kinetic region the value of ρ/ρ_s remains practically the same at $x > 5\lambda_c$. This means that we would be able to obtain about the same result if the thickness of the kinetic region is decreased by a factor of 4. In this case, the choice of the value of δ_{R_d} turns out to be a relatively simple task. Note that the vapour density jump is observed both at the droplet surface and at the outer boundary of the kinetic region. This is a typical result following from

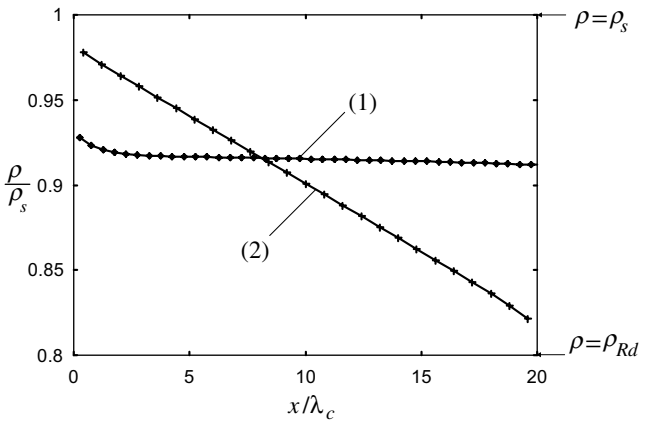

Fig. 3. Plots of normalised density of *n*-dodecane vapour ρ/ρ_s versus normalised distance from the droplet surface x/λ_c, assuming that $T_s = T_{Rd} = 600$ K, $\rho_{Rd} = 0.8\rho_s$, $\delta_{R_d} = 20\lambda_c$ and the total pressure of the mixture of vapour and air in the hydrodynamic region is equal to 3 MPa. Plot (1) refers to the case when the partial pressure of air in the kinetic region is equal to zero. Plot (2) refers to the case when the contribution of air in the kinetic region is taken into account, so that the total pressure there is equal to 3 MPa. Subscripts s and Rd refer to the droplet's surface and the outer boundary of the kinetic region respectively.

the kinetic modelling of the phenomenon (cf. [71]). The situation is rather different in the case when the presence of air is taken into account. As can be seen from Fig. 3, no saturation effect, demonstrated for the case without air, can be observed. Also, the plots of ρ/ρ_s versus x/λ_c for $\delta_{R_d} = 10\lambda_c$ and $\delta_{R_d} = 50\lambda_c$ and the same partial air pressure have been calculated. They are noticeably different from those shown in Fig. 3 for $\delta_{R_d} = 20\lambda_c$. From the point of view of practical applications, this leads to the problem of correct choice of δ_{R_d}.

A possible approach to this problem would be to take the largest possible value of δ_{R_d}. This may, however, be impractical due to excessive CPU requirements. A tenfold increase in this thickness would increase CPU time by a factor of 100.

We suggest an alternative approach, which we found useful for practical applications, based on the observation that the actual flux of vapour leaving the droplet can be found from the relationship

$$j_s = j_s^+ - j_s^-, \tag{20}$$

where j_s^+ is the flux in the x-direction at the surface of the droplet ($x = 0$), which is determined by T_s, $\rho_s(T_s)$, and the value of the evaporation coefficient β, j_s^- is the corresponding flux in the $-x$ direction. The latter is formed due to the fact that molecules of vapour emitted from the surface of the droplet collide with one another and with other molecules, and some of them return to the droplet. j_s^- is determined from the solution of the Boltzmann equations. In our analysis it will be assumed that $\beta = 1$.

When the kinetic region is thin enough, then the number of collisions in it is expected to be small and j_s^- is close to zero. The increase in δ_{R_d} leads to the increase in j_s^- and the corresponding decrease of j_s. However, at large distances from the droplet surface the effect of collisions on the returning flux diminishes and j_s^- reaches its saturation level. In this case the constant flux of vapour $j_s = j_{Rd}$ is established.

The plots of j^+ and j^- for *n*-dodecane vapour versus x/λ_c, for the same values of parameters as in Fig. 3 (curve (2)) and the total pressure of the mixture of vapour and air $p = 3$ MPa, are shown in Fig. 4a. The value of δ_{R_d} is assumed equal to $50\lambda_c$. As follows from this figure, both j^+ and j^- decrease with increasing x/λ_c, but the difference between them, $j = j_s = j_{Rd}$ (net flux), remains the same, as expected. The same plots as in Fig. 4a but for air are shown in Fig. 4b. The latter figure shows that both j^+ and j^- for air increase with increasing x/λ_c but the difference between them remains close to zero. This reflects the fact that there is no net flux of air towards droplets in steady state conditions. Small differences between j^+ and j^- for air reflect errors in computation.

Let ρ_1 and ρ_2 be vapour densities near the droplet surface and the outer boundary of the kinetic region: $\rho_1 < \rho_s$, $\rho_2 > \rho_{Rd}$ and $\rho_1 > \rho_2$ (see Fig. 3). The latter inequality results from molecular collisions. In the absence of such collisions (free molecular flow) $\rho_1 = \rho_2$. In this case $\rho_s - \rho_1$ and $\rho_2 - \rho_{Rd}$ would reach their maximum values. In the case of large numbers of collisions, gas behaves in

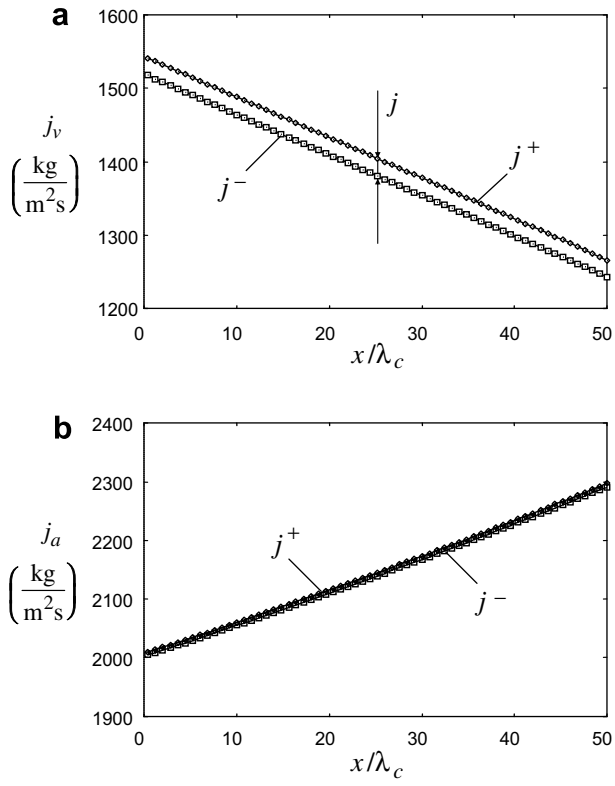

Fig. 4. Plots of j^+ and j^- versus x/λ_c for *n*-dodecane vapour (a) and air (b). The values of input parameters T_s, ρ_{Rd}, λ_c are the same as for Fig. 3 (curve (2)). δ_{R_d} is taken to be equal to $50\lambda_c$. The difference between j^+ and j^- gives the net flux for vapour (a) and air (b). The pressure of the mixture of fuel vapour and air is taken to be equal to 3 MPa.

a similar way to a continuous medium where ρ_1 is very close to ρ_s, ρ_2 is very close to ρ_{Rd} and the gradient of ρ inside the kinetic region reaches its maximal value.

Let $\Delta\rho \equiv \rho_1 - \rho_2$. We would expect that this new parameter depends on the number of collisions experienced by a molecule of vapour inside the kinetic region, $N = \delta_{R_d}/\lambda_c$, and varies between 0 and $\Delta\rho_{max} = \rho_s - \rho_{Rd}$ when N increases from 0 to ∞ (cf. [16]). This property of $\Delta\rho$ has been used in the development of the new algorithm for determination of the vapour mass flux at the outer boundary of the kinetic region. This algorithm is based on the properties of vapour density and flux illustrated in Fig. 5a, b and Fig. 6a, b.

The plots of ρ/ρ_s versus x/λ_c for various δ_{Rd} are shown in Fig. 5a. The plots for $\delta_{Rd} = 10\lambda_c$ and $\delta_{Rd} = 20\lambda_c$ have been calculated, but are not shown in this figure. It has been assumed that $p_{total} = 3$ MPa, $T_s = 600$ K and $\rho_{Rd} = 0.8\rho_s$. As follows from this figure, the curves tend to form a plateau for large x/λ_c only when $\delta_{Rd} = 250\lambda_c$. A plateau is even more clearly seen in Fig. 5b, where the plot of j versus δ_{Rd}/λ_c is shown for the same values of parameters as in Fig. 5a. As follows from Fig. 5b, j remains practically constant at $\delta_{Rd}/\lambda_c > 200$.

Combining Fig. 5a and b, we have been able to find the values of j as functions of $\Delta\rho/\rho_s$ for various δ_{Rd}. These values are shown in Fig. 6a for $\delta_{Rd} = 10\lambda_c$ (point 1), $\delta_{Rd} = 20\lambda_c$ (point 2), $\delta_{Rd} = 50\lambda_c$ (point 3), $\delta_{Rd} = 150\lambda_c$ (point 4), $\delta_{Rd} = 250\lambda_c$ (point 5). As can be seen in this figure, points 1–5 lie almost on a straight line and j can be presented as a linear function of $\Delta\rho$

$$j = -a\Delta\rho + b, \tag{21}$$

where a, b are constants depending on T_s and the partial pressure of air. The negative value of the coefficient before $\Delta\rho$ reflects the fact that j decreases when $\Delta\rho$ increases.

The predictions of Eq. (21) have been checked against the results of numerical solutions to the Boltzmann equation for evaporating n-dodecane droplets into air, assuming that the total pressures are in the range 0.2–5 MPa, $T_s = 600$ K, $\rho_{Rd} = 0.8\rho_s$ and $\rho_s(T_s) = 22.09$ kg/m^3. The results were shown to be consistent with predictions of Eq. (21). In the plots shown in Fig. 6b we restricted our analysis to $p = 3$ MPa, but considered a set of values of ρ_{Rd} in the range $0.5\rho_s$–$0.9\rho_s$. As can be seen from this figure, j is clearly a linear function of $\Delta\rho$ for the whole range of ρ_{Rd}, in agreement with Eq. (21).

Similar results were obtained for other values of T_s in the range 400–659 K (critical temperature of n-dodecane).

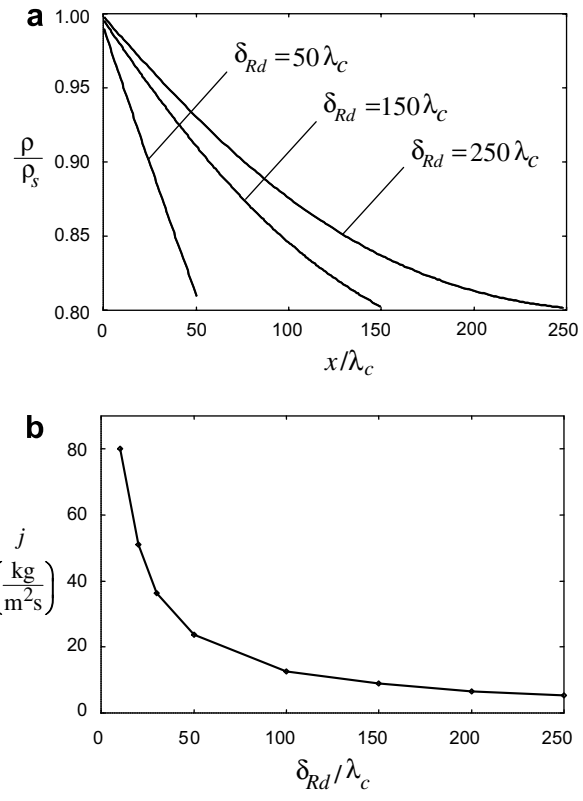

Fig. 5. The plots of ρ/ρ_s for n-dodecane vapour versus x/λ_c for various δ_{Rd} (indicated near the plots) (a) and the plot of j versus δ_{Rd}/λ_c (b). It is assumed that $p_{total} = 3$ MPa, $T_s = 600$ K and $\rho_{Rd} = 0.8\rho_s$.

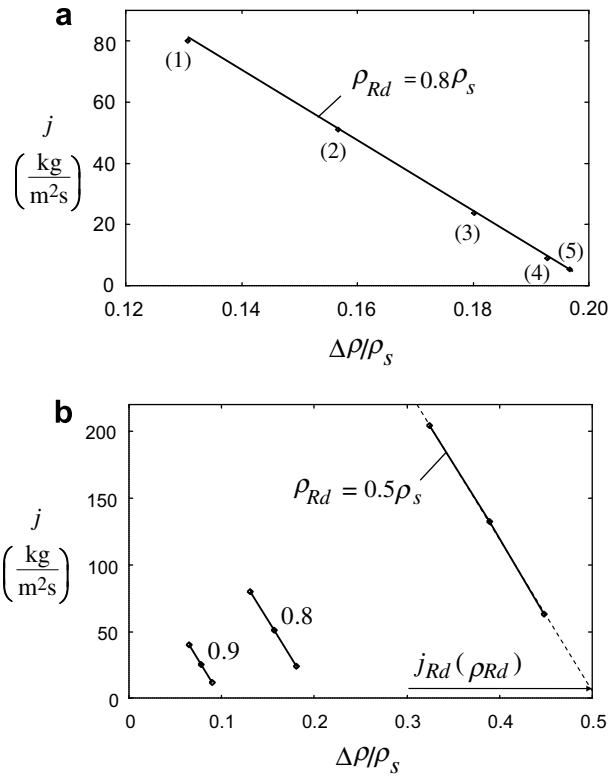

Fig. 6. The values of the net mass flux j for n-dodecane vapour as functions of $\Delta\rho/\rho_s$ for various δ_{Rd}: $\delta_{Rd} = 10\lambda_c$ (point 1), $\delta_{Rd} = 20\lambda_c$ (point 2), $\delta_{Rd} = 50\lambda_c$ (point 3), $\delta_{Rd} = 150\ \lambda_c$ (point 4) and $\delta_{Rd} = 250\lambda_c$ (point 5). These points are connected by a straight line. The values of p_{total}, T_s and ρ_{Rd} are the same as in Fig. 5a. Plots of j versus $\Delta\rho/\rho_s$ for the same p_{total} and T_s as in Fig. 5, but for various ρ_{Rd} (numbers near the lines) (b). The values of j and $\Delta\rho$ used for the latter plots were calculated for $\delta_{R_d} = 10\lambda_c$, $\delta_{R_d} = 20\lambda_c$ and $\delta_{R_d} = 50\lambda_c$. The intersection between the line corresponding to a chosen value of ρ_{Rd} and the vertical line $\Delta\rho/\rho_s = \Delta\rho_{max}/\rho_s = (\rho_s - \rho_{Rd})/\rho_s$ gives the required value of the net flux $j_{Rd}(\rho_{Rd})$. The arrow shows the value of this flux for $\rho_{Rd} = 0.5\rho_s$.

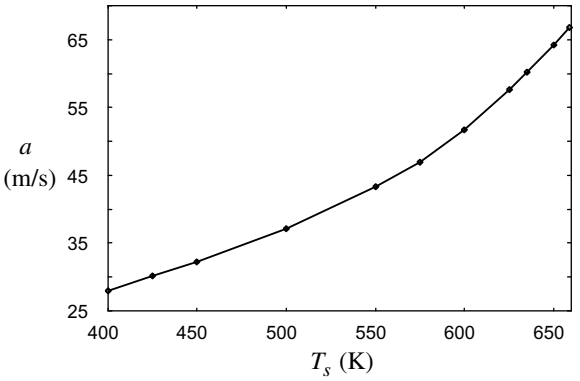

Fig. 7. The plot of a, introduced in Eq. (21), versus T_s, for the total pressure of the mixture of vapour and air equal to 3 MPa.

The plot of a versus T_s for this range of temperatures is shown in Fig. 7. As can be seen from this figure, a and its derivative increase with increasing T_s.

The plots shown in Fig. 6b are extrapolated towards higher $\Delta\rho$ and their intersections with the vertical lines corresponding to $\Delta\rho = \Delta\rho_{max}$ are found. This is expected to give the true value of j_{Rd} for the chosen value of ρ_{Rd}, since $\Delta\rho \to \Delta\rho_{max}$ when $\delta_{R_d} \to \infty$. An explicit expression for $j = j_{Rd}$ can be obtained from Eq. (21) by replacing $\Delta\rho$ with $\Delta\rho_{max}$

$$j_{Rd} = -a(\rho_s - \rho_{Rd}) + b, \tag{22}$$

where b is a function of ρ_{Rd}. From our computations (see Fig. 5) it follows that b is proportional to $\rho_s - \rho_{Rd}$, i.e. $b = c(\rho_s - \rho_{Rd})$, where c is the new constant. This allows us to rewrite Eq. (22) as

$$j_{Rd} = -\tilde{a}(\rho_s - \rho_{Rd}), \tag{23}$$

where $\tilde{a} = a - c$.

Using the set of lines shown in Fig. 6b or Eq. (23) we obtained the plots of $j(\rho_{Rd}/\rho_s) = j_s(\rho_{Rd}/\rho_s) = j_{Rd}(\rho_{Rd}/\rho_s)$ for $R_{d0} = 20$ μm and $R_{d0} = 5$ μm. These are shown in Fig. 8 (see plots (1) and (2)). In the same figure, the plots of j_{diff} versus ρ_{Rd}/ρ_s, as obtained from the mass diffusion and convection equation in the hydrodynamic region (see the right-hand side of Eq. (11)), are presented (see plots (3) and (4)). The intersection points between the two curves j_{Rd} and j_{diff}, corresponding to the same values of R_{d0}, give the values of $j_{Rd} = j_{diff}$ and the corresponding values of ρ_{Rd}. In the case shown in this figure, for $R_{d0} = 20$ μm: $j_{Rd} = j_{diff} = 0.217$ kg/(m^2 s) and $\rho_{Rd} = 0.972\rho_s$, while for $R_{d0} = 5$ μm: $j_{Rd} = j_{diff} = 0.657$ kg/(m^2 s) and $\rho_{Rd} = 0.867\rho_s$. The increase in j_{diff} when R_{d0} decreases is the expected result (see the right-hand side of Eq. (11)). Note that the finite value of δ_{R_d} (about 1 μm) is responsible for the deviation of the ratio $j_{diff}(R_{d0} = 5\ \mu m)/j_{diff}(R_{d0} = 20\ \mu m)$ from 4. The relatively weak dependence of j_{diff} on ρ_{Rd} reflects comparatively small kinetic corrections to j_{diff} despite considerable deviations of ρ_{Rd} from ρ_s. The difference between $j_{Rd}(R_{d0} = 5\ \mu m)$ and $j_{Rd}(R_{d0} = 20\ \mu m)$ is due to the contribution of the term κ_{R_d} in the left-hand side of Eq. (11). This

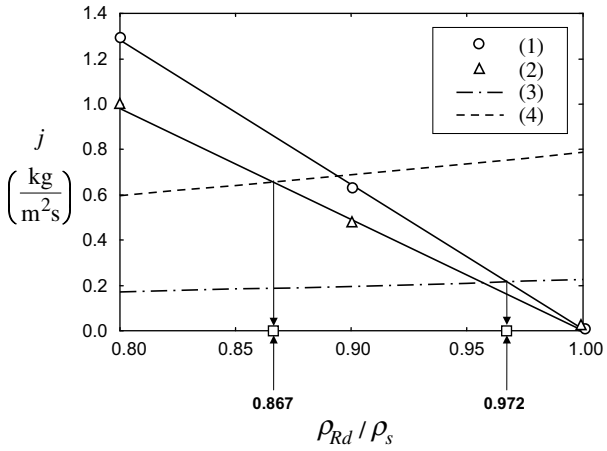

Fig. 8. Plots of fuel vapour mass flux j_{Rd} versus ρ_{Rd}/ρ_s, as obtained from Fig. 6b or Eq. (23), and fuel vapour mass flux j_{diff} versus ρ_{Rd}/ρ_s, as obtained from the mass diffusion and convection equation in the hydrodynamic region. Lines (1) and (2) refer to j_{Rd} for $R_{d0} = 20$ μm and $R_{d0} = 5$ μm respectively. Curves (3) and (4) refer to j_{diff} for $R_{d0} = 20$ μm and $R_{d0} = 5$ μm respectively. As in Fig. 6b, it was assumed that $T_s = 600$ K. The intersection points between $j_{Rd}(\rho_{Rd}/\rho_s)$ and $j_{diff}(\rho_{Rd}/\rho_s)$, corresponding to the same values of R_{d0}, give the values of $j_{Rd} = j_{diff}$ and the corresponding values of ρ_{Rd}. In the case shown in this figure, for $R_{Rd} = 20$ μm: $j_{Rd} = j_{diff} = 0.217$ kg/(m^2 s) and $\rho_{Rd} = 0.972\rho_s$. For $R_{Rd} = 5$ μm: $j_{Rd} = j_{diff} = 0.657$ kg/(m^2 s) and $\rho_{Rd} = 0.867\rho_s$.

term takes into account the difference in the areas of the droplet surface and the outer boundary of the kinetic region.

5. Results

To validate the numerical algorithm described in the previous section, a number of functionality tests and comparisons with the results reported by other authors were performed [31]. For example, Fig. 22 from [27] for number density was reproduced. In this section the model and numerical algorithm, described in the previous sections, are applied to simulate the process of heating and evaporation of a diesel fuel droplet, with initial temperature 300 K, inserted into hot air at a pressure of 3 MPa. As already mentioned, the contribution of chemical reactions between fuel vapour and oxygen is ignored. Firstly we consider a simplified problem, where the contribution of air in the kinetic region is ignored (Section 5.1). Then a more general problem, where the contribution of air is taken into account, is considered (Section 5.2).

5.1. One-component gas in the kinetic region

Let us consider the evaporation of diesel fuel droplets of various radii into a hot gas at various temperatures, using essentially the same assumptions as in [17] (only fuel vapour is present in the kinetic region). Since the value of the evaporation coefficient for diesel fuel is not known, we assumed that it was equal to 1 when the model and numerical algorithm described above were used (in contrast to [17], where it was assumed equal to the minimal and

average values of β reported for water). To characterise the evaporation process we found it convenient to introduce the new coefficient, which we called the net evaporation coefficient and defined as

$$\beta_e = \frac{j_{Rd}}{j_s^+}. \tag{24}$$

The plot of β_e versus T_s is shown in Fig. 9 by the dashed curve. As can be seen from this figure, β_e increases from about 0.0001 at $T_s \approx 450$ K to about 0.00025 at $T_s \approx 650$ K. This indicates that only a very small fraction of molecules leaving the droplet surface reaches the outer boundary of the kinetic region.

To compare the predictions of the new model and numerical algorithm and the predictions of the approximate model reported in [17] we consider the problem of evaporation of a relatively large droplet of $R_{d0} = 20$ μm into air at temperature $T_g = 650$ K (assumed to be constant during the whole process). The time evolution of normalised droplet radius and temperature, $R = R_d/R_{d0}$ and $T = T_s/T_{cr}$ ($T_{cr} = 659$ K is the critical temperature of *n*-dodecane), is shown in Fig. 10. The calculations were performed, using the model and numerical algorithm described above (solid curves 1), the hydrodynamic model (dashed–dotted curves 2), the simplified kinetic models with $\beta = 1$ (dashed curves 3) and with $\beta = 0.04$ (dotted curves 4). As follows from this figure, the curves, predicted by the kinetic model based on the direct numerical solution of the Boltzmann equation (rigorous kinetic model), the simplified kinetic model based on $\beta = 1$ and $\beta = 0.04$, and the hydrodynamic model, almost coincide. The reduction in the evaporation time predicted by the hydrodynamic model and the simplified kinetic model with $\beta = 1$ and $\beta = 0.04$, when compared with the rigorous kinetic model, is less than 1% and can be ignored in most practical applications.

Similar results were obtained for $R_{d0} = 5$ μm and other values of gas temperature ($T_g = 750$ K and $T_g = 1000$ K)

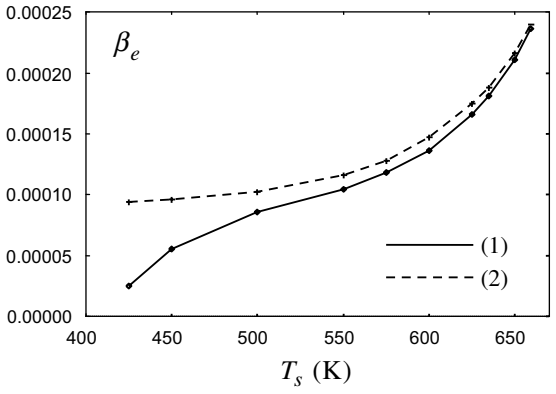

Fig. 9. Plots of the net evaporation coefficient β_e, as predicted by Eq. (24), versus T_s, assuming that the total pressure is equal to 3 MPa. The solid curve (1) refers to the case when the contribution of air in the kinetic region is taken into account. The dashed curve (2) refers to the case when the contribution of air in this region is ignored.

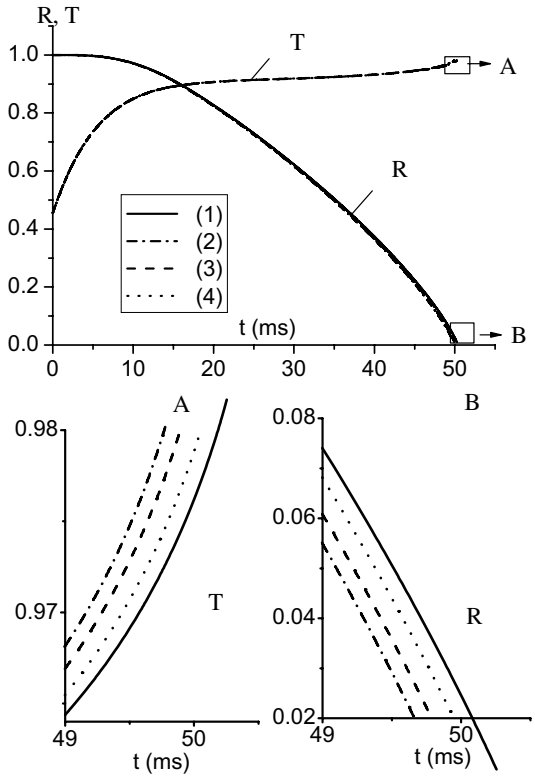

Fig. 10. Plots of $R = R_d/R_{d0}$ and $T = T_s/T_{cr}$ versus time, as predicted by the rigorous kinetic model (1), hydrodynamic model (2), simplified kinetic model with $\beta = 1$ (3) and simplified kinetic model with $\beta = 0.04$ (4). The total pressure is 3 MPa, the initial droplet temperature is 300 K, $R_{d0} = 20$ μm, $T_g = 650$ K and $T_{cr} = 659$ K. The contribution of air in the kinetic region is ignored.

for both initial droplet radii. These results seem to cast doubt over the conclusion drawn in [17], that kinetic effects lead to noticeable increase in droplet evaporation time in the case of diesel fuel droplet evaporation into a high pressure gas. The application of the conventional hydrodynamic model, almost universally used in computational fluid dynamics (CFD) codes, seems to be vindicated. This conclusion, however, was based on the assumption that only fuel vapour is present in the kinetic region. A more general problem, when the contribution of air in the kinetic region is taken into account, is considered in the next subsection.

5.2. Two-component gas in the kinetic region

Let us now consider the same problem as in Section 5.1, but take into account the presence of air in the kinetic region. The partial pressure of air is found as

$$p_a = p_{total} - p_v, \tag{25}$$

where p_v is the actual partial pressure of fuel vapour.

As in the case of one-component gas in the kinetic region considered in Section 5.1, we assumed that the evaporation coefficient β was equal to 1. Also, as in the case of the one-component gas, the values of the net evaporation

coefficient β_e as functions of the droplet surface temperature were calculated directly using the rigorous kinetic model and Eq. (24). The results are shown in Fig. 9 by the solid curve. It can be seen from this figure that the values of β_e in the presence of air are noticeably smaller when compared with the case of one-component gas in the kinetic region. For example, in the case when $T_s < 450$ K the values of β_e in the presence of air are less than half of those predicted for the case when the contribution of air in the kinetic region is ignored. At the qualitative level this could be expected if we take into account the increased role of collisions in the kinetic region in the presence of air. As in the case without air in the kinetic region, the value of β_e increases with increasing surface temperature.

Plots of $R = R_d/R_{d0}$ and $T = T_s/T_{cr}$ versus time are shown in Figs. 11–16 for various initial droplet radii and gas temperatures. These were calculated using three models:

(a) the kinetic model based on the direct numerical solution of the Boltzmann equation, described in the previous sections (rigorous kinetic model) (solid curves 1);
(b) the hydrodynamic model (dashed–dotted curves 2);
(c) the kinetic model based on the approximate solution [17] with $\beta = 1$ (dashed curves 3).

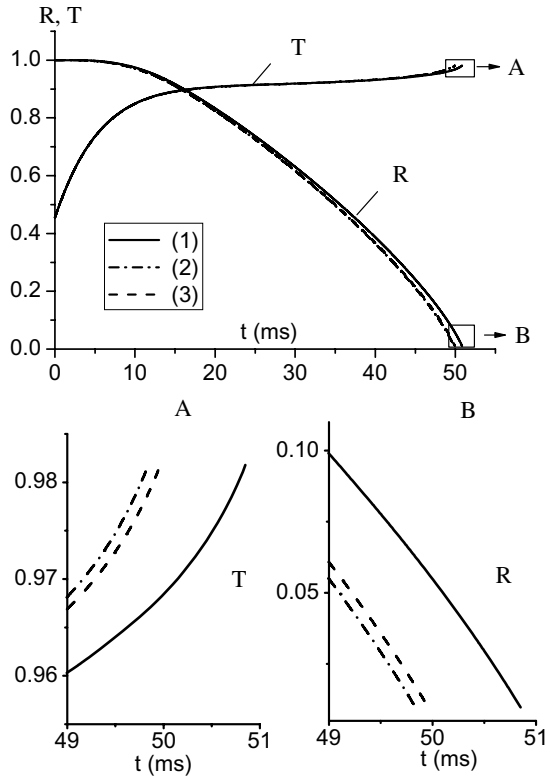

Fig. 11. Plots of $R = R_d/R_{d0}$ and $T = T_s/T_{cr}$ versus time, as predicted by the rigorous kinetic model (1), hydrodynamic model (2), and simplified kinetic model with $\beta = 1$ (3). The total pressure is 3 MPa, the initial droplet temperature is 300 K, $R_{d0} = 20$ μm and $T_g = 650$ K. The contribution of air in the kinetic region is taken into account.

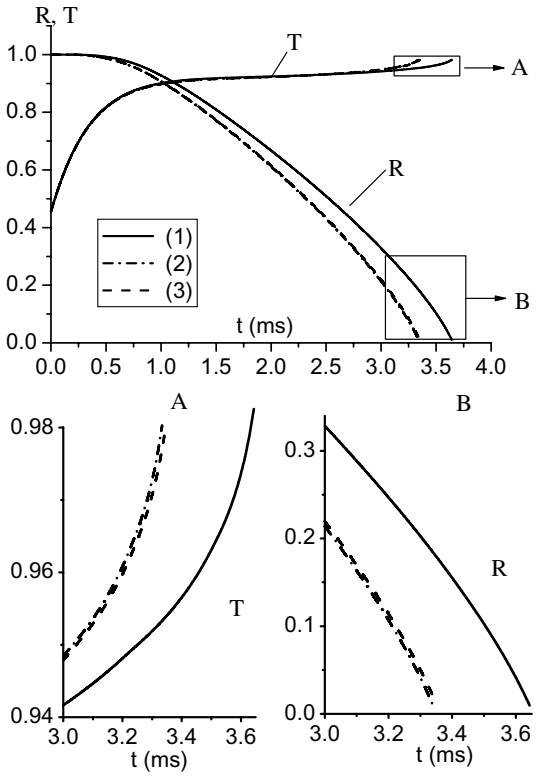

Fig. 12. The same as Fig. 11 but for $R_{d0} = 5$ μm.

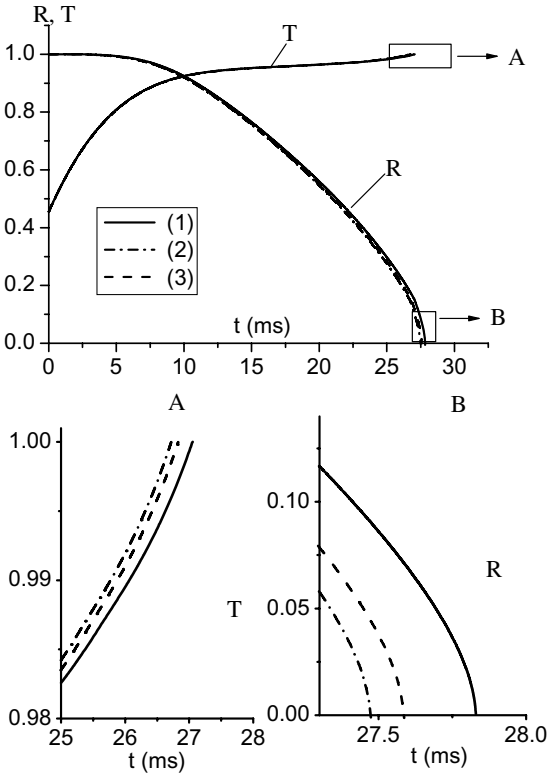

Fig. 13. The same as Fig. 11 but for $T_g = 750$ K.

All these figures show that the hydrodynamic model always overpredicts the value of droplet surface tempera-

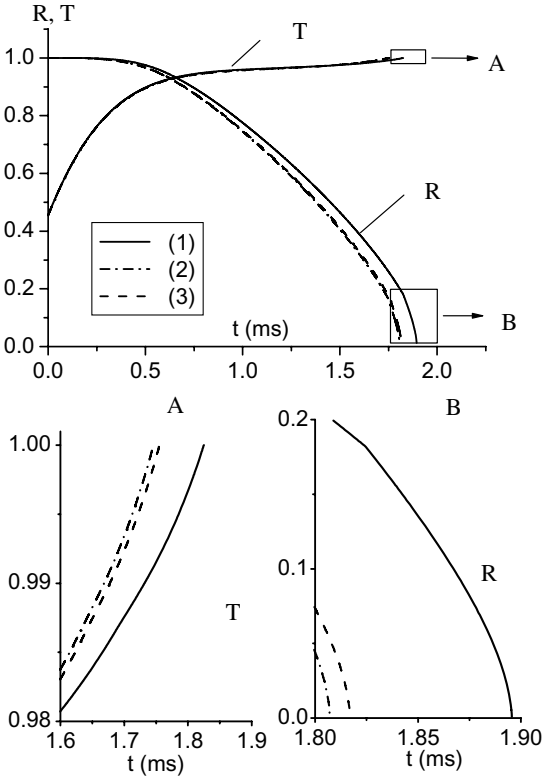

Fig. 14. The same as Fig. 12 but for $T_g = 750$ K.

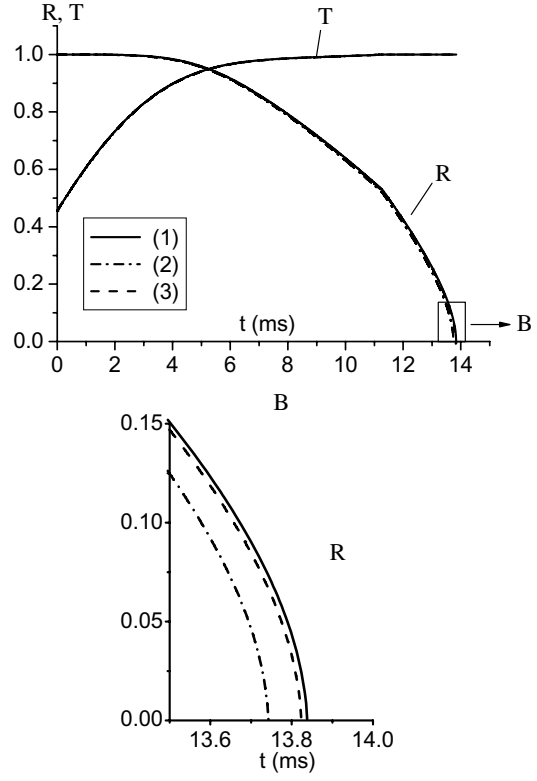

Fig. 15. The same as Fig. 11 but for $T_g = 1000$ K.

ture and underpredicts the values of droplet radii and evaporation times, as expected (this result is compatible with the one shown in Fig. 10 for the case of the one-component gas in the kinetic region). The values of droplet surface temperature and radius, predicted by the simplified kinetic model with $\beta = 1$, always lie between those predicted by the hydrodynamic model and the rigorous kinetic model.

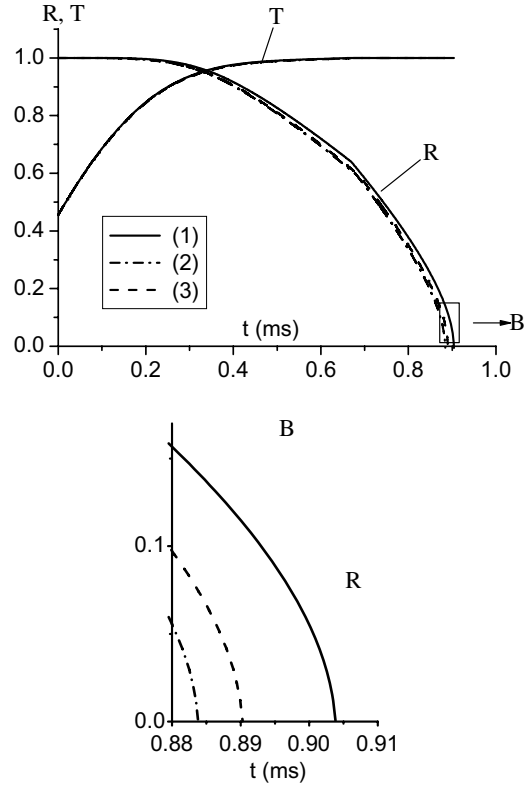

Fig. 16. The same as Fig. 12 but for $T_g = 1000$ K.

Note that in some cases the difference between the predictions of the simplified and rigorous kinetic models is negligible (e.g. see Fig. 15). In other cases, however, this difference is noticeable and needs to be taken into account. To quantify the accuracy of the models we introduced the following parameter:

$$E = \frac{\tau_{\text{evap}}^{\text{RK}} - \tau_{\text{evap}}^{\text{M}}}{\tau_{\text{evap}}^{\text{RK}}} \times 100\%, \tag{26}$$

where $\tau_{\text{evap}}^{\text{RK}}$ is the evaporation time (time during which the droplet radius reduces from its initial value to zero) predicted by the rigorous kinetic model, $\tau_{\text{evap}}^{\text{M}}$ is the evaporation time predicted by the model under consideration (simplified kinetic or hydrodynamic), E is the relative error of prediction of the model under consideration, in percent. The results of the estimation of E for the hydrodynamic and simplified kinetic model are shown in Table 1.

As follows from this table, the errors in predictions of the hydrodynamic model always increase with decreasing initial droplet radii and decreasing gas temperatures. The maximal error of 8.3% was recorded for $R_{d0} = 5$ μm and $T_g = 650$ K. The smallest error of 0.7% was recorded for $R_{d0} = 20$ μm and $T_g = 1000$ K. The errors in prediction

Table 1
The values of E for simplified kinetic and hydrodynamic models

R_{d0} (μm)	20	5	20	5	20	5
T_g (K)	650	650	750	750	1000	1000
E (simplified kinetic)	1.7%	8.0%	0.9%	4.1%	0.1%	1.5%
E (hydrodynamic)	2.0%	8.3%	1.3%	4.7%	0.7%	2.2%

of the simplified kinetic model are always less than those for the hydrodynamic model. As follows from our calculations, the decrease in errors, E, with increasing temperature leads to the situation when these errors are negligibly small for $T_g > 1000$ K. In the case of $R_{d0} = 20$ μm and $T_g = 2000$ K the predictions of the simplified and rigorous kinetic models almost coincide. In the case of $R_{d0} = 5$ μm and $T_g = 2000$ K the simplified model predicts the evaporation time about 1.2% less than the rigorous model.

Note that some differences in the results obtained using the simplified model presented in this paper and in [17] can be attributed to smaller values of β and the different diffusion model used in [17]. Also, the effect of curvature of the droplets and the outer boundary of the kinetic region were totally ignored in [17].

6. Conclusions

A new kinetic model for droplet evaporation into a high pressure background gas (air) is described. This model is based on the introduction of the kinetic region around evaporating droplets, where the dynamics of molecules is described in terms of the Boltzmann equations for vapour and air. The boundary condition at the outer boundary of the kinetic region is introduced by matching the mass fluxes of vapour leaving the kinetic region and entering into the surrounding hydrodynamic region. The collisions between vapour molecules, air molecules, and air and vapour molecules in the kinetic region are taken into account. The numerical algorithm used for the solution of the Boltzmann equations is essentially based on the approach suggested by Aristov and Tcheremissine [24]. The matching condition for molecular fluxes at the outer boundary of the kinetic region is found based on the observation that the net mass flux of evaporating molecules j is proportional to the difference in the density of the saturated fuel vapour corresponding to the droplet surface temperature and the fuel vapour density near the outer boundary of the kinetic region.

The model and numerical algorithm described above allow us to calculate the value of the net evaporation coefficient β_e. This coefficient is defined as the ratio of the actual flux leaving the outer boundary of the kinetic region to the maximal possible flux leaving the droplet surface. Using the values of parameters typical for diesel engines (total pressure 3 MPa), it is shown that the values of β_e increase from about 0.0001 to 0.00025 when droplet surface temperature increases from about 450 K to approximately 650 K, for the case when the contribution of air in the kinetic region is ignored. When the contribution of air is taken into account, β_e increases from about 0.00005 to 0.00025 for the same range of droplet surface temperatures. In contrast to the results reported in [17] based on the simplified kinetic model, the kinetic effects predicted by the model and numerical algorithm described above are negligible when the contribution of air in the kinetic region is ignored.

This effect, however, appears to be noticeable if the contribution of air in the kinetic region is taken into account. In this case, the underprediction of the droplet evaporation time by the hydrodynamic model compared with the rigorous kinetic model, described in this paper, increases when droplets' initial radius R_{d0} and gas temperature T_g decrease. For $R_{d0} = 5$ μm and $T_g = 650$ K this underprediction was more than 8%. The predictions of the droplet evaporation time and surface temperature by the simplified kinetic model almost always lie between those for the hydrodynamic model and the rigorous kinetic model. The application of the rigorous kinetic model, as described in this paper, is recommended when accurate predictions of the values of droplet surface temperature and evaporation time are essential.

Acknowledgements

The authors are grateful to the EPSRC (Grants EP/C527089/01 and EP/E02243X/1) (UK) and the Russian Foundation for Basic Research (Grant No. 06-08-81013) (Russia) for the financial support of this project. Our special thanks go to Professor G. Nagayama for drawing our attention to her papers [40,43] and useful discussions of theoretical estimates of the evaporation coefficient.

References

[1] H. Hertz, Über die Verdunstung der Flussigkeiten, inbesondere des Quecksilbers, im lufteeren Raume, Ann. Phys. Chem. 17 (1882) 177–200.
[2] M. Knudsen, Die maximale verdampfungsgeschwindigkeit des quecksilbers, Ann. Phys. 47 (1915) 697–708.
[3] R.W. Schrage, A Theoretical Study of Interface Mass Transfer, Columbia University Press, New York, 1953.
[4] N.A. Fuchs, The evaporation and growth of droplets in a gaseous medium, in: Progress in Science and Engineering, Academy of Science of the USSR Publishing House, Moscow, 1958 (in Russian).
[5] E.M. Lifshitz, L.P. Pitaevski, Physical Kinetics, Nauka Publishing House, Moscow, 1979.
[6] R.I. Nigmatulin, Dynamics of Multiphase Media, vol. 1, Hemisphere Publishing Corporation, 1991.
[7] V. Chernyak, The kinetic theory of droplet evaporation, J. Aerosol. Sci. 26 (1995) 873–885.
[8] J. Rose, Interphase matter transfer, the condensation coefficient and dropwise condensation, in: Proceedings of 11th International Heat

Transfer Conference, August 23–28, 1998, Kyongji, Korea, vol. 1, 1998, pp. 89–104.
[9] A.B. Kozyrev, A.G. Sitnikov, The evaporation of a spherical droplet into a moderate-pressure gas, Uspekhi (Progr. Phys. Sci.) 171 (2001) 725–734.
[10] A Lotfi, Molekulardynamische simulationen an fluiden: phasengleichgewicht und verdampfung, Dissertation zur Erlangung des akademischen Grades Doktor-Ingenieur der Fakultät für Maschinenbau der Ruhr-Universität Bochum, Bochum, 1993.
[11] V.S. Galkin, M.N. Kogan, O.G. Fridlender, Some kinetic effects in continuum flows, Fluid Dyn. 5 (1970) 364–371.
[12] M.N. Kogan, N.K. Makashev, On the role of the Knudsen layer in the theory of heterogeneous reactions and flows with the surface reactions, Reports of the Academy of Sciences of USSR. Mech. Liquids Gases 6 (1971) 3–11 (in Russian).
[13] Y. Sone, K. Aoki, S. Takata, H. Sugimoto, A.V. Bobylev, Inappropriateness of the heat-conduction equation for description of a temperature field of a stationary gas in the continuum limit: examination by asymptotic analysis and numerical computation of the Boltzmann equation, Phys. Fluids 8 (1996) 628–638, 8 (1996) 841–841 (E).
[14] Y. Sone, S. Takata, H. Sugimoto, On the behaviour of a gas in the continuum limit in the light of kinetic theory: the case of cylindrical Couette flows with evaporation and condensation, Phys. Fluids 8 (1996) 3403–3413, 10 (1998) 1239–1239 (E).
[15] Y. Sone, Kinetic Theory and Fluid Dynamics, Birkhäuser, Springer, 2002.
[16] S. Takata, K. Aoki, Two-surface problems of a multicomponent mixture of vapors and noncondensable gas, Phys. Fluids 11 (1999) 2743–2756.
[17] A.P. Kryukov, V.Yu. Levashov, S.S. Sazhin, Evaporation of diesel fuel droplets: kinetic versus hydrodynamic models, Int. J. Heat Mass Transfer 47 (2004) 2541–2549.
[18] W.A. Sirignano, Fluid Dynamics and Transport of Droplets and Sprays, Cambridge University Press, 1999.
[19] S.S. Sazhin, Advanced models of fuel droplet heating and evaporation, Progr. Energy Combust. Sci. 32 (2006) 162–214.
[20] T.M. Muratova, D.A. Labuntsov, Kinetic analysis of the evaporation and condensation processes, Therm. Phys. High Temp. 7 (1969) 959–967 (in Russian).
[21] P.F. Flynn, R.P. Durrett, G.L. Hunter, A.O. zur Loye, O.C. Akinyemi, J.E. Dec, C.K. Westbrook, Diesel combustion: an integrated view combining laser diagnostics, chemical kinetics, and empirical validation, SAE report 1999-01-0509, 1999.
[22] E.M. Sazhina, S.S. Sazhin, M.R. Heikal, V.I. Babushok, R. Johns, A detailed modelling of the spray ignition process in Diesel engines, Combust. Sci. Technol. 160 (2000) 317–344.
[23] K. Aoki, C. Bardos, S. Takata, Knudsen layer for gas mixtures, J. Statist. Phys. 112 (2003) 629–655.
[24] V.V. Aristov, F.G. Tcheremissine, Direct Numerical Solution of the Boltzmann Equation, Computer Centre of Russian Academy of Sciences, Moscow, 1992.
[25] F.G. Tcheremissine, Conservative evaluation of Boltzmann collision integral in discrete ordinates approximation, Comput. Math. Appl. 35 (1998) 215–221.
[26] F.G. Tcheremissine, Discrete approximation and examples of the solution of the Boltzmann equation, in: Computational Dynamics of Rarefied Gases, Computer Centre of Russian Academy of Sciences, Moscow, 2000, pp. 37–74.
[27] K. Aoki, S. Takata, S. Kosuge, Vapor flows caused by evaporation and condensation on two parallel plane surfaces: effect of the presence of a noncondensable gas, Phys. Fluids 10 (1998) 1519–1534.
[28] S. Taguchi, K. Aoki, S. Takata, Vapor flows condensing at incidence onto a plane condensed phase in the presence of noncondensable gas. I. Subsonic condensation, Phys. Fluids 15 (2003) 689–705.
[29] S. Taguchi, K. Aoki, S. Takata, Vapor flows condensing at incidence onto a plane condensed phase in the presence of noncondensable gas. II. Supersonic condensation, Phys. Fluids 16 (2004) 79–92.
[30] A.P. Kryukov, V.Yu. Levashov, I.N. Shishkova, Condensation in the presence of a non-condensable component, J. Eng. Phys. Thermophys. 78 (2005) 15–21 (in Russian).
[31] I.N. Shishkova, S.S. Sazhin, A numerical algorithm for kinetic modelling of evaporation processes, J. Comput. Phys. 218 (2006) 635–653.
[32] M.N. Kogan, Rarefied Gas Dynamics, Plenum, New York, 1969.
[33] V.M. Zhdanov, M.Ya. Alievskii, Transport and Relaxation Processes in Molecular Gases, Nauka Publishing House, Moscow, 1989 (in Russian).
[34] V.Ya. Rudiak, On the theory of kinetic equations for dense gases, J. Techn. Phys. 54 (1984) 1246 (in Russian); English translation is available.
[35] Yu.L. Klimontovich, Kinetic Theory of Non-ideal Gas and Non-ideal Plasma, Nauka Publishing House, Moscow, 1975 (in Russian).
[36] L.D. Landau, E.M. Lifshitz, Theoretical Physics, Mechanics, vol. 1, Nauka Publishing House, Moscow, 1965 (in Russian).
[37] A.P. Kryukov, V.Yu. Levashov, I.N. Shishkova, Flows of vapour–gas mixtures in micro- and nano-systems in the presence of evaporation and condensation, in: Proceedings of the 4th Russian National Heat Transfer Conference, Moscow, 2007, vol. 1, pp. 164–167 (in Russian).
[38] J.B. Maxwell, Data Book on Hydrocarbons: Application to Process Engineering, D. van Nostrand Company, Inc., New York, 1950.
[39] S. Maruyama, Molecular dynamics method for micro/nano systems, in: W.J. Minkowycz, E.M. Sparrow, J.Y. Murthy (Eds.), Handbook of Numerical Heat Transfer, John Wiley & Sons, 2006 (Chapter 21).
[40] T. Tsuruta, G. Nagayama, Molecular dynamics studies on the condensation coefficient of water, J. Phys. Chem. B 108 (2004) 1736–1743.
[41] V. Carravetta, E. Clementi, Water–water interaction potential: an approximation of the electron correlation contribution by a functional of the SCF matrix, J. Chem. Phys. 81 (1984) 2646–2651.
[42] H.J.C. Berendsen, J.R. Grigera, T.P. Straatsma, The missing term in effective pair potential, J. Phys. Chem. 91 (1987) 6269–6271.
[43] G. Nagayama, T. Tsuruta, A general expression for the condensation coefficient based on transition state theory and molecular dynamic simulation, J. Chem. Phys. 118 (2003) 1392–1399.
[44] G. Gladstone, K.J. Laidler, H. Eyring, The Theory of Rate Processes, McGraw-Hill, New York, 1941.
[45] R.B. Bird, W.E. Stewart, E.N. Lightfoot, Transport Phenomena, John Wiley & Sons, 2002.
[46] J.O. Hirschfelder, C.F. Curtiss, R.B. Bird, Molecular Theory of Gases and Liquids, John Wiley & Sons, 1954.
[47] A.H. Lefebvre, Atomization and Sprays, Taylor & Francis, 1989.
[48] I.S. Grigoriev, E.Z. Meilikhov (Eds.), Handbook of Physical Quantities, CRC Press, 1996, pp. 427–430.
[49] C. Cercignani, Theory and Application of the Boltzmann Equation, Scottish Academic Press, Edinburgh, London, 1975.
[50] B. Abramzon, W.A. Sirignano, Droplet vaporization model for spray combustion calculations, Int. J. Heat Mass Transfer 32 (1989) 1605–1618.
[51] S.S. Sazhin, P.A. Krutitskii, W.A. Abdelghaffar, E.M. Sazhina, S.V. Mikhalovsky, S.T. Meikle, M.R. Heikal, Transient heating of diesel fuel droplets, Int. J. Heat Mass Transfer 47 (2004) 3327–3340.
[52] S.S. Sazhin, W.A. Abdelghaffar, E.M. Sazhina, M.R. Heikal, Models for droplet transient heating: effects on droplet evaporation, ignition, and break-up, Int. J. Therm. Sci. 44 (2005) 610–622.
[53] B. Abramzon, S. Sazhin, Droplet vaporization model in the presence of thermal radiation, Int. J Heat Mass Transfer 48 (2005) 1868–1873.
[54] B. Abramzon, S. Sazhin, Convective vaporization of fuel droplets with thermal radiation absorption, Fuel 85 (2006) 32–46.
[55] S.S. Sazhin, W.A. Abdelghaffar, P.A. Krutitskii, E.M. Sazhina, M.R. Heikal, New approaches to numerical modelling of droplet transient heating and evaporation, Int. J. Heat Mass Transfer 48 (2005) 4215–4228.

[56] S.S. Sazhin, T. Kristyadi, W.A. Abdelghaffar, M.R. Heikal, Models for fuel droplet heating and evaporation: comparative analysis, Fuel 85 (2006) 1613–1630.
[57] S.S. Sazhin, P.A. Krutitskii, S.B. Martynov, D. Mason, M.R. Heikal, E.M. Sazhina, Transient heating of a semitransparent spherical body, Int. J. Therm. Sci., in press.
[58] L.A. Dombrovsky, S.S. Sazhin, Absorption of thermal radiation in a semi-transparent spherical droplet: a simplified model, Int. J. Heat Fluid Flow 24 (2003) 919–927.
[59] L.A. Dombrovsky, S.S. Sazhin, Absorption of external thermal radiation in asymmetrically illuminated droplets, J. Quant. Spectrosc. Radiat. Transfer 87 (2004) 119–135.
[60] L.A. Dombrovsky, Absorption of thermal radiation in large semi-transparent particles at arbitrary illumination of a polydisperse system, Int. J. Heat Mass Transfer 47 (2004) 5511–5522.
[61] C.C. Tseng, R. Viskanta, Effect of radiation absorption on fuel droplet evaporation, Combust. Sci. Technol. 177 (2005) 1511–1542.
[62] A.P. Kryukov, V.Yu. Levashov, I.N. Shishkova, A.K. Yastrebov, The Numerical Solution of the Boltzmann Equation for Engineering Applications, Moscow Power Engineering Institute Publishing House, Moscow, 2005.
[63] H.K. Versteeg, W. Malalasekera, An Introduction to Computational Fluid Dynamics, Longman, 1999.
[64] N.S. Bakhvalov, N.P. Zhidkov, G.M. Kobelkov, Numerical Methods, Nauka Publishing House, Moscow, 1989 (in Russian).
[65] N.M. Korobov, Trigonometric Sums and Their Applications, Nauka Publishing House, Moscow, 1989 (in Russian).
[66] F.G. Tcheremissine, Conservative method for the solution of the Boltzmann equation for centrally symmetrical interaction potentials, Reports of Russian Academy of Science 357 (1997) 53–56 (in Russian).
[67] S.P. Popov, F.G. Tcheremissine, Conservative method for the solution of the Boltzmann equation for centrally symmetrical interaction potentials, Comput. Math. Math. Phys. 39 (1999) 163–176.
[68] T. Imamuro, B. Sturtevant, Numerical study of discrete-velocity gases, Phys. Fluids 2 (1990) 2196–2203.
[69] F. Rogier, J.A. Schneider, A direct method for solving the Boltzmann equation, Transp. Theory Statist. Phys. 23 (1994) 1–3.
[70] C. Buet, S. Cordier, P. Degond, Regularized Boltzmann operators, Comput. Math. Appl. 35 (1998) 55–74.
[71] S.S. Sazhin, V.V. Serikov, Rarefied gas flows: hydrodynamic versus Monte Carlo modelling, Planet. Space Sci. 45 (1997) 361–368.